The Egyptian Journal of Remote Sensing and Space Sciences 22 (2019) 49–58

HOSTED BY

Contents lists available at ScienceDirect

The Egyptian Journal of Remote Sensing and Space Sciences

journal homepage: www.sciencedirect.com

Research Paper

Downscaling of MODIS thermal imagery

Kishan Singh Rawat [a,b,*], V.K. Sehgal [a], S.S. Ray [c]

[a] Division of Agricultural Physics, Indian Agricultural Research Institute, New Delhi 110012, India
[b] Sathyabama Institute of Science and Technology (SIST), (Deemed to be University), Chennai-600119 (T.N.), India
[c] Mahalanobis National Crop Forecast Centre (MNCFC), Pusa Campus, New Delhi 110012, India

ARTICLE INFO

Article history:
Received 18 January 2017
Revised 28 November 2017
Accepted 9 January 2018
Available online 20 December 2018

Keywords:
Downscaling
TsHARP
TPS
MODIS
LANDSAT-7

ABSTRACT

In this paper, integration of two models TsHARP (Tsharp) and Thin plate spline (TPS) has been performed for spatial sharpening of 1 km (coarse) resolution of MODIS thermal imagery to 250 m resolution. Afterwards it was validated with LANDSAT-7 thermal data (after resampled to 250 m pixel). The results showed that LST based on integration of two (TsHARP and TPS) models is consistent with true data (LANDSAT-7 ETM+, thermal data). We have observed R^2 at pure cropped area, cropped area with low settlement and cropped area with high settlement is showing, 0.74 (Multi R = 0.80, Adju R = 0.75 and p = .001), 0.72 (Multi R = 0.78, Adju R = 72 and p = .001) and 0.71 (Multi R = 0.78, Adju R = 0.71 and p = .001) respectively. While overall R^2 of 0.69 (Multi R = 0.76, Adju R = 0.71 and p = .000) for all categories of classes (cropped area + cropped area with low settlement + cropped area with high settlement). LST shows root mean square error (RMSE) = 0.307 °C, Relative-RMSE (R-RMSE) = 0.167 °C, mean absolute error (MAE) = 0.033 °C, normalized RMSE (NRMSE) = 0.018 °C, index of agreement (d) = 0.99, RMSE-observations standard deviation ratio (RSR) = 0.39 and RMSE% = 0.02 for merging process based LST. We conclude that combination of TsHARP and TPS model has a great potential to estimate LST at 250 m with high temporal resolution. This LST can be used as an input in various models to estimate other components which are LST dependent.

1. Introduction

Temperature information is required for crop and agriculture monitoring at fine scale for analysis and their anticipated impacts. Readily available LST's data at global (with coarse spatial scale) and higher temporal scale (per day) are provided by some satellite (MODIS). These LST data most of time, do not fit to the needs of local/sub-local adaptation planning due to only poor spatial resolution (SR). Therefore, decision makers are interested in alternate of fine SR with high temporal resolution LST data sets for specific sectors, e.g., agricultural and hydrology.

A remote sensing (RS) technique provides a unique opportunity to capture land surface information over large geographic extents at different resolutions. Therefore satellite data at finer scale is essential for various applications. Mathematically it is possible to make same spatial resolution of different spatial resolution data from same satellite source. MODIS has different spatial resolution (250, 500 and 1000 m) data sets from optical/thermal sensor at same temporal resolution. Another issue is mismatch of optical and thermal data sets at fine scale (optical data at 250 m) and thermal data at 1 km). Results from analysis of different scale of bands (optical and thermal) without downscaling of thermal band with respect to optical band cannot be reliable therefore it is necessary that both bands must be in same spatial and temporal scale. Such types of data have a good temporal resolution (per day) and can be used for near real time monitoring of crop parameters. MODIS data sets have high temporal resolution (per day) but both bands have different SR (250 m optical and 1000 m thermal band). This type of disparity between two different kinds of SR bands can be removed using mathematical models like TsHARP and TSP.

TsHARP method is robust and widely accepted due to its powerful functioning and simplicity (Zhan et al., 2013). The powerful functioning of TsHARP is based on the fact that vegetation covers, mainly represented by combination of NIR (Near Infrared Region) and Red band based vegetation index (VI) known as Normalized Difference Vegetation Index (NDVI). It is the most significant key for determining the land surface temperature (LST) of many landscapes. Therefore, this model has a sole assumption that LST (from

Peer review under responsibility of National Authority for Remote Sensing and Space Sciences.
* Corresponding author.
E-mail address: kr_rawat2002@yahoo.com (K. Singh Rawat).

https://doi.org/10.1016/j.ejrs.2018.01.001
1110-9823/

thermal band) and NDVI (from optical band) is associated with a unique relationship across a given sensor scene (data sets) and free from different SR scales.

However, recent research work reports some of the deficiencies of TsHARP method. The different scale effect of the LST-NDVI relationship cannot always be disregarded, which could lead to a sizeable error for areas dominated by natural covered area by vegetation (Chen et al., 2012b). Moreover, NDVI is not only single factor that determines LST. This suggests that LST govern by other factors (e.g., Soil moisture (SM), albedo) also in areas where NDVI values are low. Although this problem can be rectified to some extent using residual correction, it is still a major source of errors for TsHARP in mixed areas (Agam et al., 2007a,b). Therefore disadvantage of TsHARP is its limitation over those areas where low NDVI exists. Therefore, TsHARP method also cannot be used as it is. This weakness of TsHARP can be removed, if we integrate TsHARP model with another model that can use the effectiveness of TsHARP at low NDVI area.

The TPS is formally known as laplacian smoothing splines and is a deterministic non-geostatistical surface fitting process. It entitles to adjust a set of function that interpolate source point data (any parameter of geo-data sets) while minimizing the smoothness term. This smoothness term represents a negotiation between the curvature of surface and the distance with source point data and is calculated by iteratively minimizing the generalized cross validation function. TPS is considered as a powerful and precise method for source point data, fine smoothness and robustness. Accordingly, TPS has been commonly used in spatial interpolation of point data (this point data may be geo-data, DEM, meteorological data, etc. (Boer et al., 2001; Chen and Li, 2012a). Previous research works have suggested the need of integration of these two model for improved spatial resolution of LST products (Yang et al., 2011; Galianoa et al., 2012; Teggi and Despini, 2014; Wang et al., 2015). Objective of this study is to integrate TPS with TsHAPR for downscaling of 1 km LST into 250 m LST.

2. Materials and methods

2.1. Study area description

Study area lies between 76° 29′ E to 76° 44′ E and 28° 17′ N to 28° 36′ N, with altitude 245 m above m.s.l. in Rewari district state of Haryana in India (Fig. 1a & b), which covers almost entire study area in which Wheat (during Rabi season) is the major crop. The average rainfall in last ten years in the district is 569.6 mm. The rainfall distribution in the district is uneven and scattered which results into drought that affects the agriculture production as well as cropping pattern in Kharif and Rabi season.

2.2. Data acquisition

Images were acquired on 19-January-2013 with MODIS systems in order to acquire optical and thermal band. The specification of MODIS data are given in Table 1. The ground-truth work was performed on 19-January-2013.

A LANDSAT-7ETM+ data of study area was acquired on 19-January-2013 and used as high resolution LST (60 m) imagery with respect to merged model data. LANDSAT-7ETM+ data have ziz-zag lines (or zero value area, due to malfunctioning of the scan line corrector).Correction operation was not necessary if selected ground truth points lies in the middle of the scene area where there is no image distortion (Bala et al., 2016).

Ground survey was conducted on same day of satellite pass over the study area. Observation (X and Y co-ordinates) were taken in different land use/land cover (LULC) types, such as fallow land, barren land, vegetation and near of water bodies/wetlands etc., were identified and their co-ordinates were logged with a hand held Global Position System (GPS) device (Garmin (eTrexH), with ± 15 m horizontal locational accuracy (Rawat et al., 2016). These data were used for validation of LANDSAT-7ETM+, LST with estimated LST from purposed merged model.

2.2.1. Data processing

2.2.1.1. Data pre-processing for temperature retrieval. In this study, for LST retrieval from LANDSAT-7ETM+ data requires radiometric calibration, atmospheric correction and emissivity estimation, prior to LST estimation. Radiometric calibration of LANDSAT-7ETM+ was done using Landsat Calibration tool in ENVI 4.5 S/W, atmospheric correction done using FLAASH module (or algorithm) in ENVI. LST was calculated (from LANDSAT-7ETM+) using standard emissivity method suggested by Zareie et al. (2016).

ArcGIS-10.2 software was used to process the MODIS data set (MOD09AQ and MOD09GQ, (Fig. 1a)). The software converts the .hdf files format into .img format. While converting the data format, its projection (spheroid_Sinusoidal) also converted into WGS_1984_Transverse_Mercator projection. Finally, after the process masking the data with fixed rectangular polygon (Fig. 1b), the analysis was limited to rectangular area. General Information of data sets is given in Table 1. Vegetation index is calculated from MOD09 reflectance products. NDVI is the normalized ratio of the NIR and the red bands, these NDVI index is calculated as Bala et al. (2016, 2015) and Rawat et al. (2012).

2.2.1.2. Resampling of LANDSAT data. Resampling is just changing of the spatial resolution of raster dataset and set rules for aggregating values across the new pixel size (250 m). In our case, nearest neighbour method was sleeted because of maximum possible spatial error is one-half the cell size (Borra-Serrano et al., 2015; it is lesser than other methods). In the present study, the Thermal band (60 m, Band 6 (TIR)) of Landsat-7 ETM+ was resample into 250 m for validation of simulated LST data (based on TsHARP and TPS).

2.3. Model

TsHARP and TPS two model were used for solving downscaling (1 km to 250 m) of thermal data (1 km) using Red (250 m) and NIR band (250 m) reflectance. Both models have advantage and disadvantage, TsHARP is fit for those area where vegetation condition is good and TPS performances is just opposite good performances at low vegetations cover area therefore in present study we merge/combine TsHARP and TPS models and use advantages of each model.

The detailed methodology used for downscaling of LST using combination/merging process is given in Fig. 2.

2.3.1. TsHARP model

TsHARP assumes that the sole relationship exists between LST and VI within a RS data at multiple spatial resolutions (like 250, 500 and 1000 m). In first step of TsHARP, establish an empirical relationship between coarse resolution NDVI (Fig. 3a) and LST (Fig. 4a).

$$\begin{aligned} T_{low} &= f_{reg}(VI) + \delta_{reg} \\ &= a * NDVI_{low} + b + \delta_{reg} \end{aligned} \quad (1)$$

where, f_{reg} *is* regression function, VI is NDVI, low suffix is represent to poor resolution (here low = 1 km SR) image, a and b are represent regression parameter, δ_{reg} residual field at poor resolution (1km) image pixel. Obtained regression equation applied over high resolution (250 m) NDVI images (Fig. 3b) and calculated high resolution (250 m) LST (or $T_{high} = T_{reg}$) as:

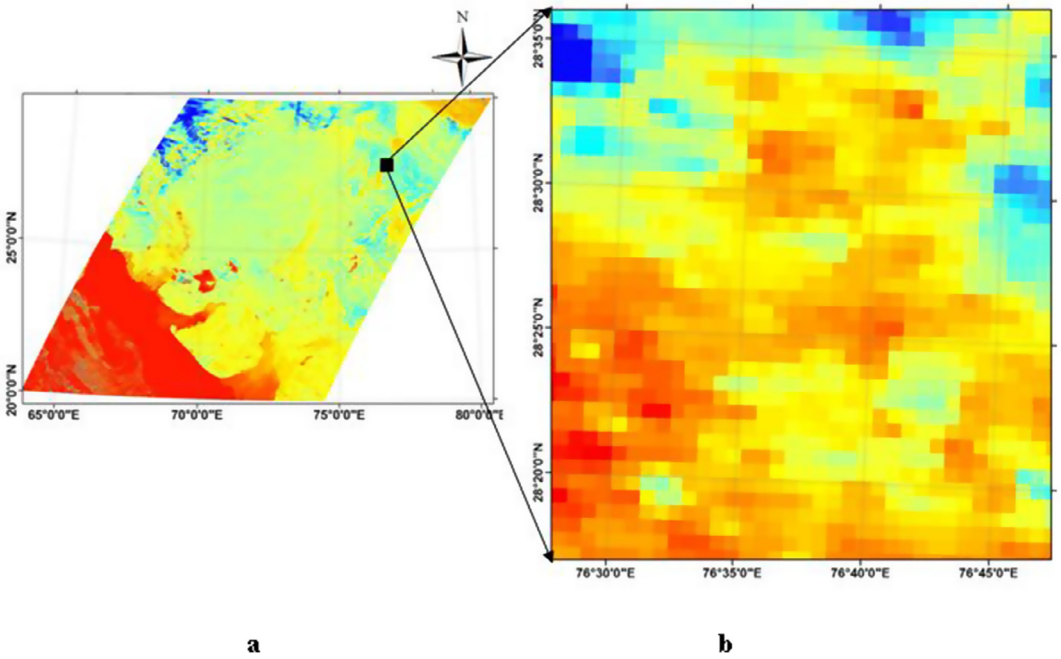

Fig. 1. a MODIS tiles, b Study area after masking from MODIS tiles.

Table 1
General information about LANDSAT-7 and MODIS data sets.

Sensor (LANDSAT-7ETM+)	Wavelength	Spectral Resolution
Band 1 (Blue)	435–520 nm	30 m
Band 2 (Green)	500–624 nm	30 m
Band 3 (Red)	614–704 nm	30 m
Band 4 (NIR)	740–914 nm	30 m
Band 5 (SWIR)	1508–1791 nm	30 m
Band 6 (TIR)	1040–1250 nm	60* (30)
Band 7	209–235 nm	30 m
Band 8	052–090 nm	15 m
Sensor (MODIS), (MOD09AQ and MOD09GQ)		
Band 1 (VIR)	620–670 nm	250 m, 500 m, 1 km
Band 2 (NIR)	841–876 nm	250 m, 500 m, 1 km
Band 3 (VIS)	459–479 nm	250 m, 500 m, 1 km
Band 4 (NIS)	545–565 nm	250 m, 500 m, 1 km
Band 5 (SWIR)	1230–1250 nm	250 m, 500 m, 1 km
Band 6 (SWIR)	1628–1652 nm	250 m, 500 m, 1 km
Band 7 (SWIR)	2105–2155 nm	250 m, 500 m, 1 km

* ETM + Band 6 is acquired at 60-meter resolution, but products are resampled to 30-meter pixels.

$$T_{high\_reg} = a * NDVI_{high} + b \tag{2}$$

Finally high resolution LST from TsHARP (Fig. 4b) is given by adding residual field (δ_{reg}) behind of regression estimate (Eq. (1)) as:

$$\begin{aligned} T_{TsHARP} &= T_{high\_reg} + \delta_{reg} \\ &= T_{high\_reg} + T_{low} - T_{reg} \\ &= T_{low} + a[NDVI_{low} - NDVI_{high}] \end{aligned} \tag{3}$$

2.3.2. TSP model

TPS is a deterministic non-geostatistical surface fitting process or in simple term it is interpolation method for known point data sets, which is commonly use able technique for downscaling of geo-data in raster format (Fig. 4c). The fundamental principle of TPS technique is based on the spatial dependence of geo-data (Bindhu et al., 2013). A general form of TPS model is given as:

$$f_{TPS} = a_{\circ} + a_1 x + a_2 y + \frac{1}{2}\sum_{i}^{n} b_i r_i^2 \log r_i^2 \tag{4}$$

with the following condition:

$$\sum_{i=1}^{n} b_i = \sum_{i=1}^{n} b_i x_i = \sum_{i=1}^{n} b_i y_i = 0 \tag{5}$$

where, $r_i^2 = (x - x_i)^2 + (y - y_i)^2$ and the parameters are obtained by satisfying the condition:

$$f_{low\_TPS} = T_{low} \tag{6}$$

$$T_{\mathrm{TPS\_high}} = f_{\mathrm{high\_TPS}} \tag{7}$$

Finally, in comparison of TsHARP method, TPS reveal less spatial details of LST image; however, it can perform better result in the areas where NDVI poor/low indicates LST.

2.4. Integration of TPS and TsHARP models

From above section it is clear that both models are just opposite in performances for NDVI condition. One (TsHARP) is highly effective in good NDVI cover area while second model (TPS) performs better in those area where NDVI cover is poor. Therefore we merge both the models to obtain a model that can perform well under good vegetation cover area as well as under week vegetation cover area. In this direction, First step, two high resolution (250 m) LST images were acquired by regression (Eq. (2) TsHARP not including δ) and TPS method, respectively. Second step, estimation of error in both method for each poor resolution pixel. Third step, the weighted results of the regression and TPS method were combined with the estimation of their errors. Finally and fourth step, δ fields were added back to the weighted results. Mathematically representations of above four steps are given as below:

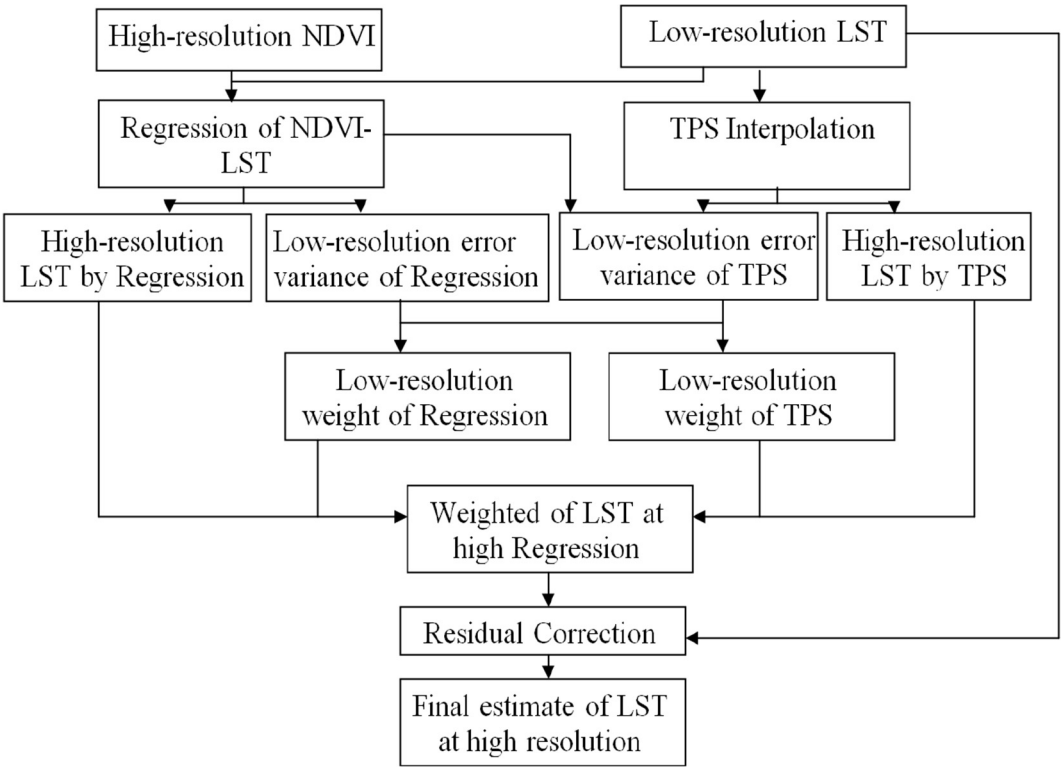

Fig. 2. Flow chart for adopted methodology.

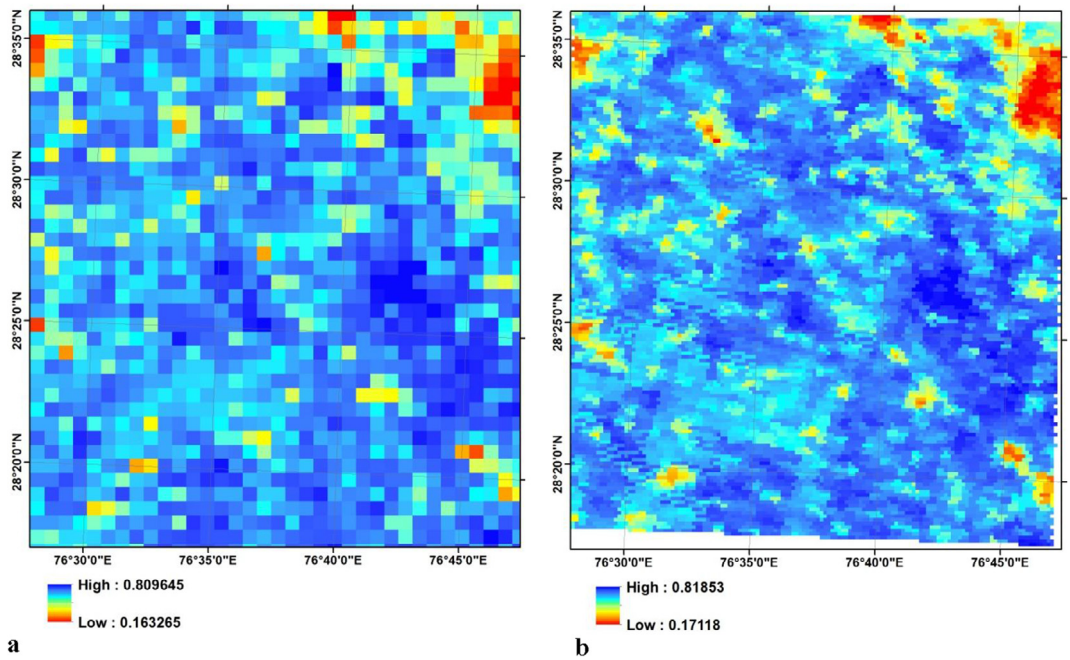

Fig. 3. a MODIS 1 km NDVI (low SR), b MODIS 250 m NDVI (high SR).

2.4.1. Mathematical representations of error estimation in regression method

For the regression method, the error variance of regressed LST in poor resolution image can be calculated as the square of a poor resolution δ (Fig. 5a) if the error is assumed to be constant in poor resolution image.

$$\delta_{reg}^2 = [T_{low} - T_{reg}]^2 \quad (8)$$

2.5. Mathematical representations of error estimation in TPS method

In most of cases, TPS produces smoother raster output with a lack of spatial information because TPS considered only spatial dependence. Therefore, the spatial variance of downscaled LST by TPS is generally lower than that of original LST (without interpolated) at same spatial resolution. Assuming that total variance (Var.) of original LST can be divided into error Var. and model

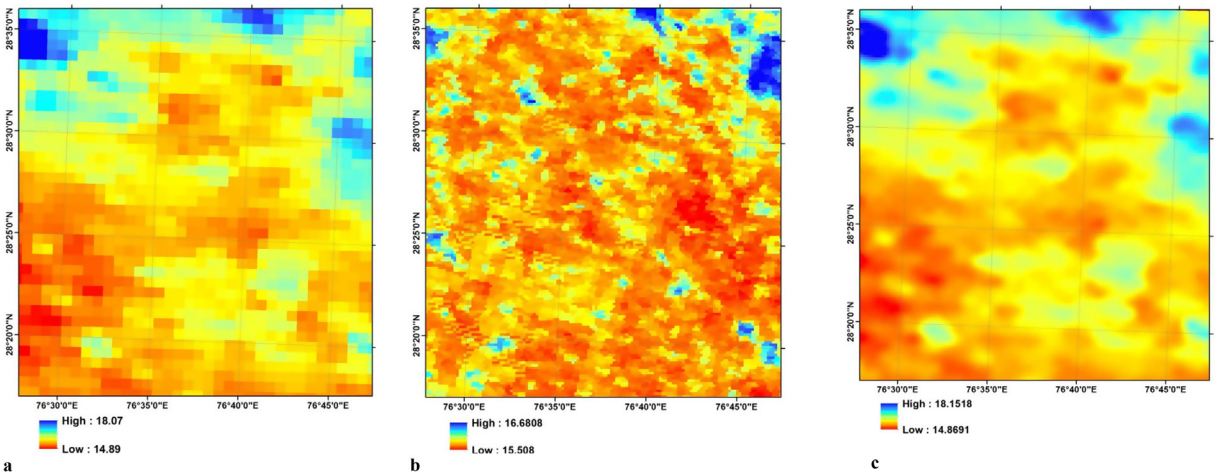

Fig. 4. a MODIS 1 km LST (low SR), b MODIS 250 m LST (T_{high_reg}), c Interpolated LST (250 m, T_{TPS_high}) using TPS.

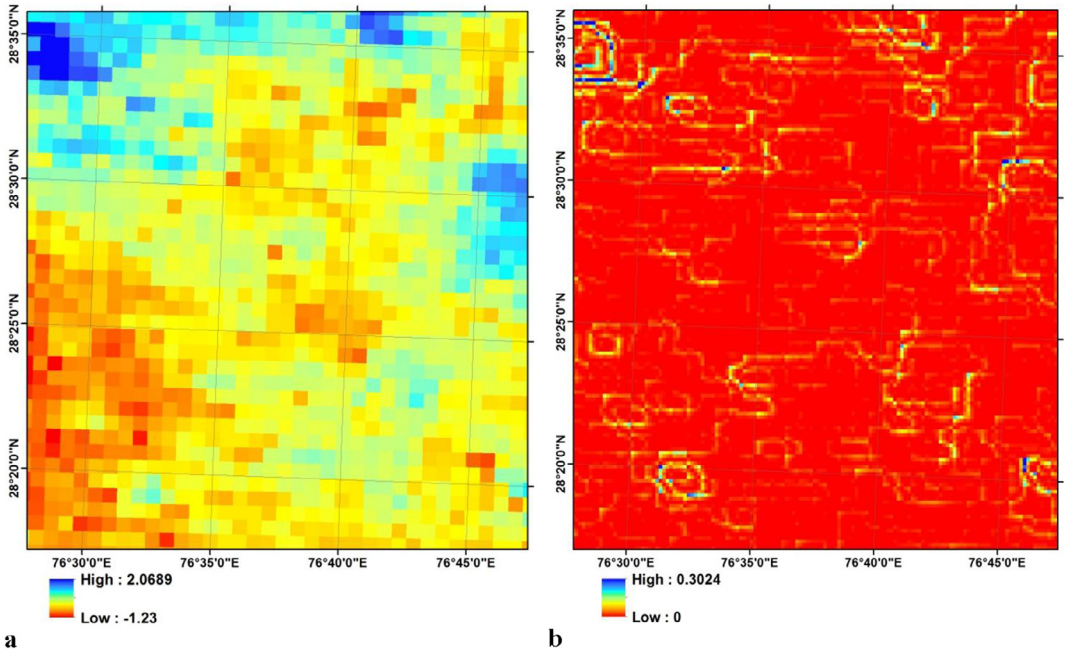

Fig. 5. a Error variance (δ^2_{reg}) of regressed LST, b variance in TPS ($Var[T_{TPS}]$).

Var., the error Var. of sharpened LST in poor resolution image can be expressing as Eq. (9):

$$\delta^2_{TPS} = |Var[T_{high} - Var[T_{TPS\_high}]| \quad (9)$$

where,

$$Var[T_{high}] = \frac{1}{m}\sum_{1}^{m}[T_{high} - T_{low}]^2 \quad (10)$$

$$Var[T_{TPS}] = \frac{1}{m}\sum_{1}^{m}[T_{TPS\_high} - T_{low}]^2 \quad (11)$$

Eq. (10) and (11, Fig. 5b) are the total Var. and model Var. of LST in poor resolution image respectively. The absolute operation in Eq. (9) is to address the abnormal case that total Var. is less than model Var. as the original high resolution LST (T_{high}) is unknown, the total Var. cannot be calculated directly. However, it can be calculated by regression between LST-NDVI and mathematically expressed as:

$$Var[T_{high}] = b^2 * Var[NDVI_{high}] + Var(\delta_{reg}) \quad (12)$$

$$Var[NDVI_{high}] = \frac{1}{m}\sum_{1}^{m}[NDVI_{high} - NDVI_{low}]^2 \quad (13)$$

and $Var(\delta_{reg})$ is the residual Var. in low/poor SR image based on LST-NDVI regression model. Now Eq. (8) can be re-write with the help of Eqs. (10), (12) (Fig. 6a) and (14) (Fig. 6b) for error Var. of TPS at each low/poor resolution image (Fig. 7a) is:

$$\delta^2_{TPS} = |b^2 * Var[NDVI_{low}] + Var(\delta_{reg}) - Var[T_{TPS\_high}]| \quad (14)$$

Eq. (14) represents Var. Difference of the LST estimated from LST-NDVI model and TPS can reflect the error of TPS. In general, spatial Var. of the LST sharpened by TPS is relatively small. If NDVI Var. in a lower resolution image is large, TPS method cannot give better output because NDVI is use as main factor to sharpening low resolution LST. But NDVI Var. is small, TPS perform better

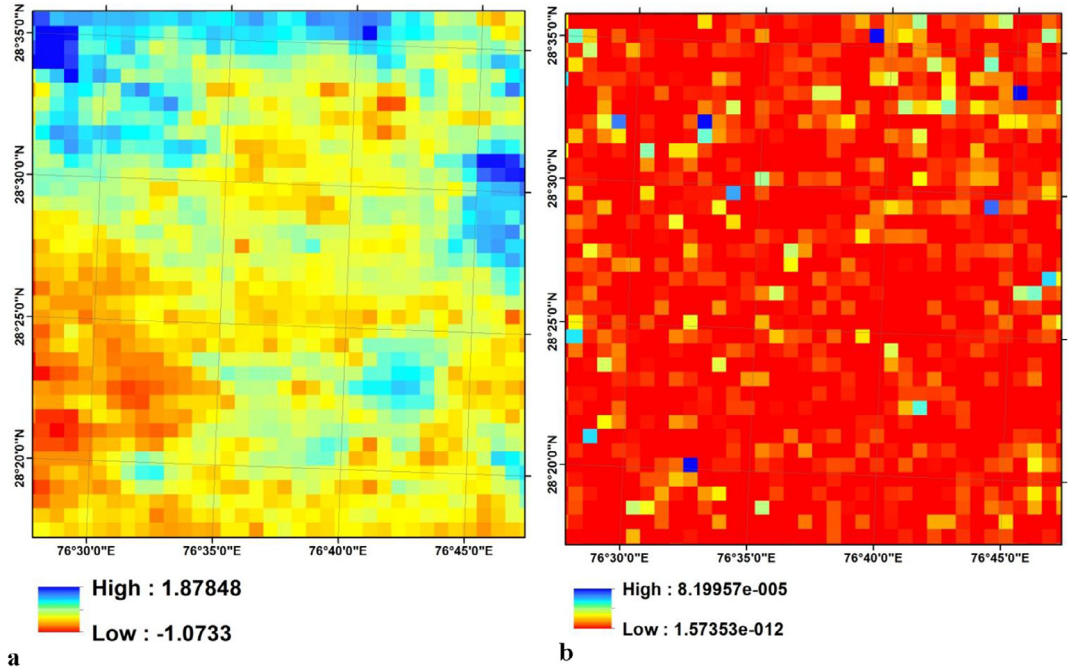

Fig. 6. a variance in T_{high} (Var[T_{high}]), b variance in $NDVI_{high}$ (Var[$NDVI_{high}$]).

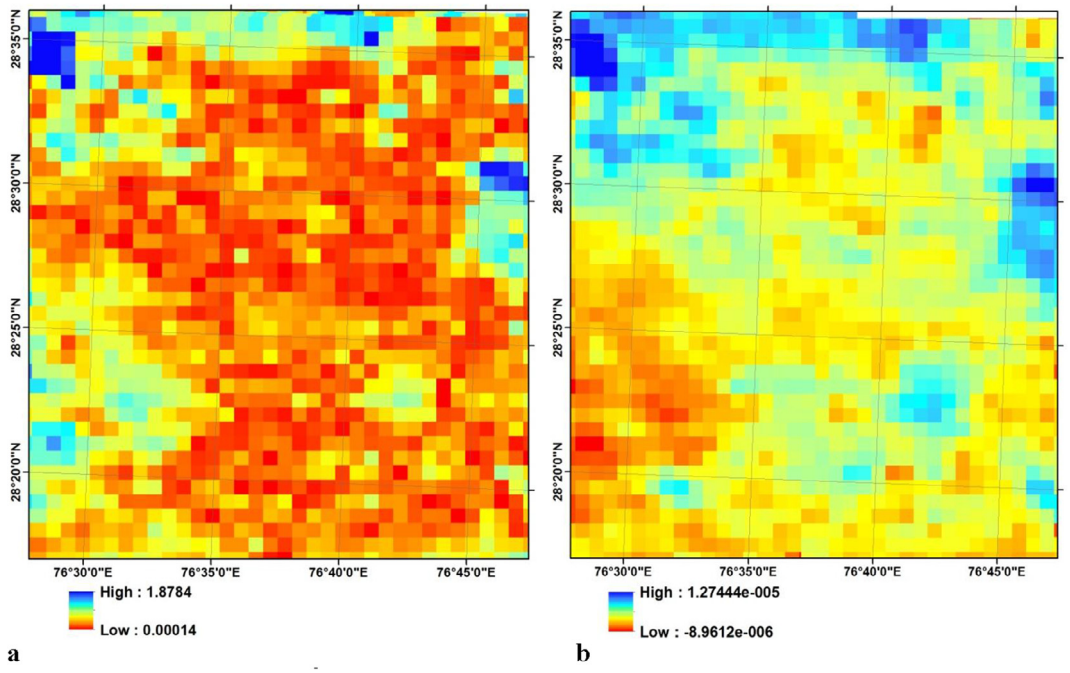

Fig. 7. a Error variance (δ^2_{TPS}) of regressed LST, b weights map per pixel (W_{TPS}).

because spatial dependency participate more important role than NDVI in estimating LST. Mainly, low/poor NDVI covered area, LST-NDVI relationship not works strongly therefore spatial dependence should be considered more.

2.6. Mathematical representations of merging TPS and TsHARP models

From Eqs. (8) and (14) we calculated sharpening error Var. of TsHARP and TPS, the weights (W_{TPS} and W_{TsHARP}) of these two models are estimated for low resolution images at pixel level as Eq. ((15), Fig. 7b) and ((17), Fig. 8a).

$$W_{TPS}(x_i, y_i) = \frac{\delta^2_{reg}(x_i, y_i)}{\delta^2_{reg}(x_i, y_i) + \delta^2_{TPS}(x_i, y_i)} \tag{15}$$

$$W_{reg}(x_i, y_i) = \frac{\delta^2_{TPS}(x_i, y_i)}{\delta^2_{reg}(x_i, y_i) + \delta^2_{TPS}(x_i, y_i)} \tag{16}$$

According to bayesian theory, weighted summation of both model (TsHARP and TPS) is the best estimation (Wikle et al., 2007). As suggestion of Wikle et al. (2007), weighted value from each modal for each lower resolution pixels must be multiple with

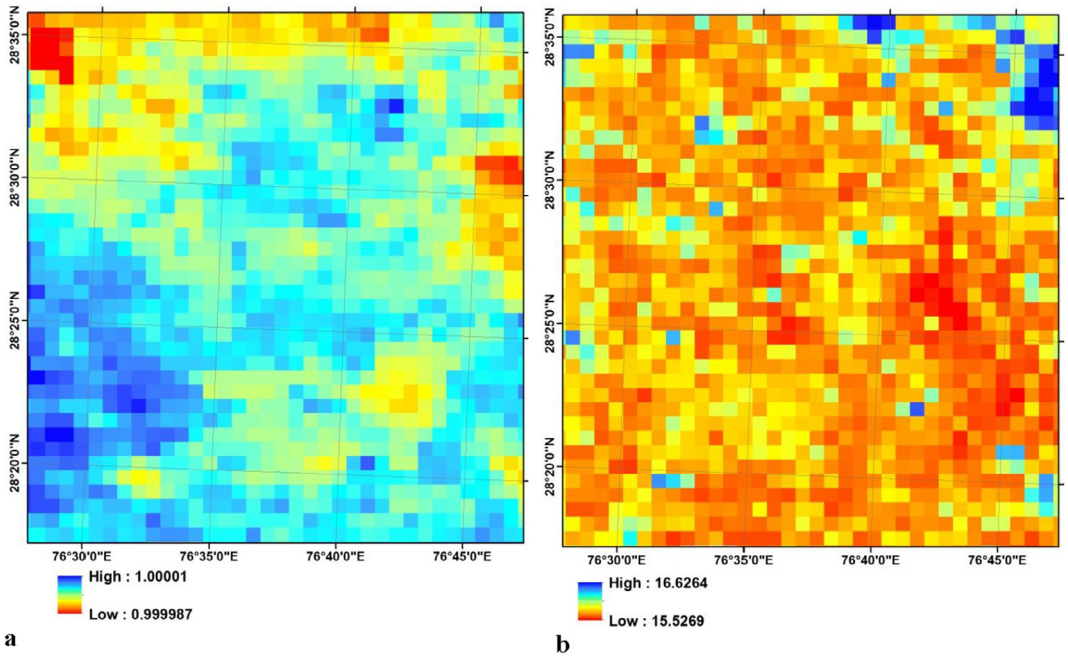

Fig. 8. a weights map per pixel (W_{reg}), b weight map (T_{weight_high}) of higher resolution image at pixel level.

generated/obtain high resolution images (T_{TSP_high} and T_{high_reg}) from both model. From Eqs. (15) and (17) a higher resolution weighted T (say T_{weight}) can be generated (Fig. 8b), which tell weight of higher resolution image at pixel level.

$$T_{Weight\_high} = W_{TPS} \times T_{TPS\_high} + W_{reg} \times T_{reg\_high} \quad (17)$$

Finally we can obtain merged high resolution LST (Fig. 9a) using TsHARP and TSP, after correction in low resolution δ field is added back to the result which is representing as:

$$T = T_{Weight\_high} + T_{low} - \frac{1}{m}\sum_{1}^{m} T_{Weight\_high} \quad (18)$$

Adopted methodology of merging or combining of TPS and TsHARP illustrated by Fig. 2.

3. Validation of merged LST data with true LST from LANDSAT-7ETM+

120 ground points at different condition (pure cropped area (C_1), cropped area with light settlements (C_2), cropped area with high settlement (C_3) and union of all class (C_4) were collected during (19th January 2013) satellites (MODIS and LANDSAT-7 (Fig. 9b)) pass over study area. We observed LST in different land use/land cover because we assumed that this range is more

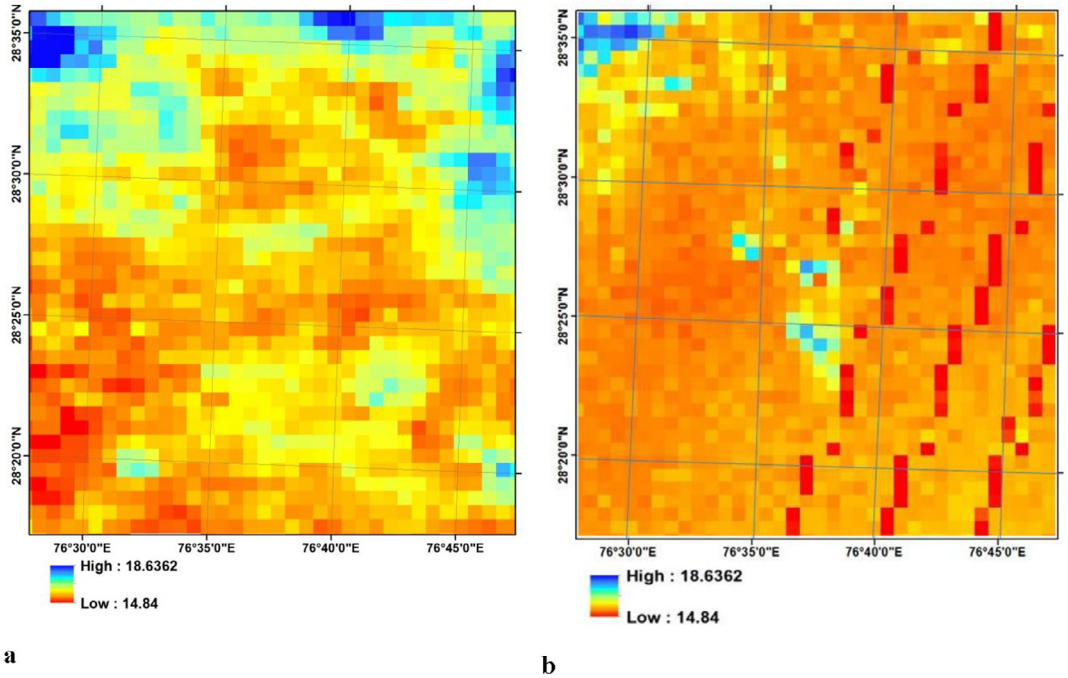

Fig. 9. a Merged high resolution (250 m) LST, b LST from LANDSAT-7ETM + using emissivity method.

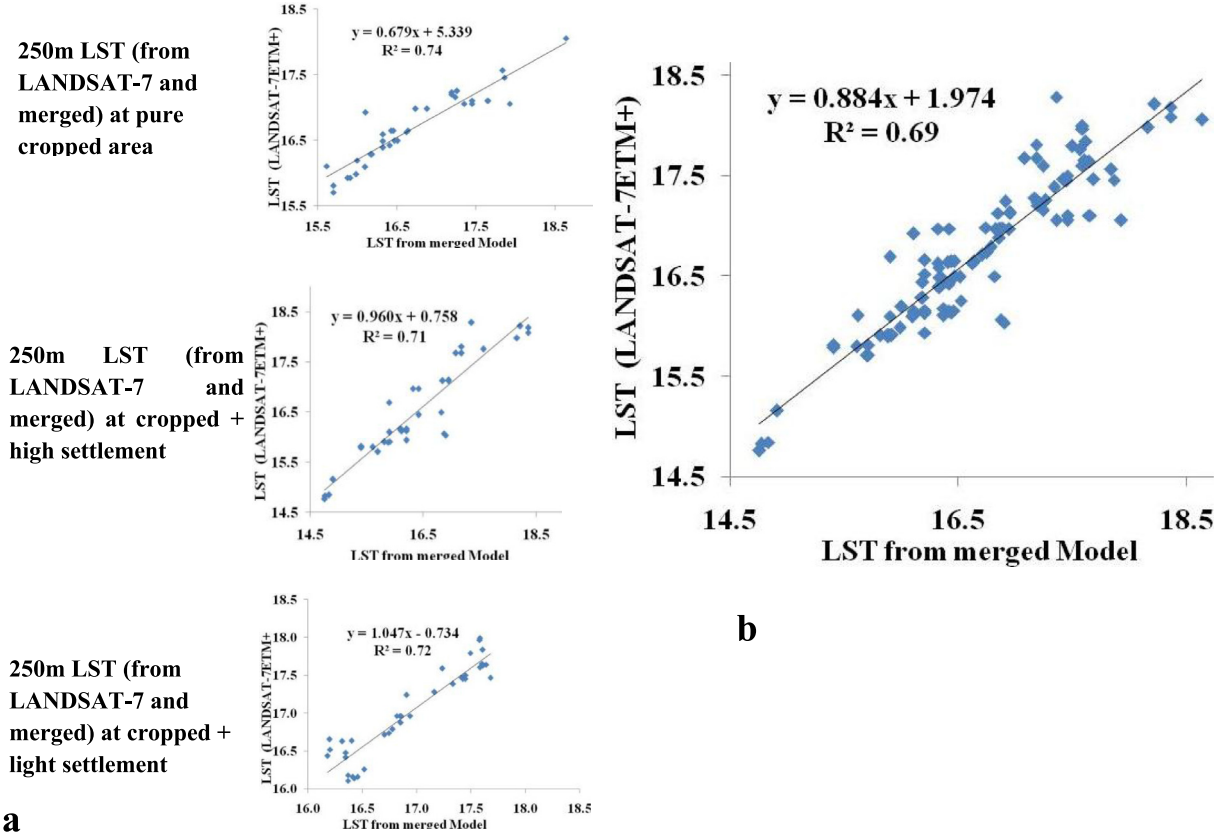

Fig. 10. Correlation between a 250 m LST from LANDSAT-7 and fused under 40 observed point data in each different category of land use and b 250 m LST (from LANDSAT-7 and merged) under full observed point data sets.

dynamic from LST point of view. LST along these points from true imagery (from LANDSAT-7 at 250 m) and purposed merged model were collected and obtain R^2 (for different condition of land use/land cover) using 2D scatter plot (Fig. 10). Another statistical test (RMSE, R-RMSC, RSR, NRMSE, MAE, and d also applied over these LST points for validation of LST from merging of two models with reference to LAND SAT-7ETM+LST.

4. Results and discussion

4.1. Downscaling

The main objective of this study was to produce daily LST at 250 m scale (Fig. 9a) identical to the MODIS MOD09GQ using combination of two models (TsHARP and TPS). The LST (at 250 m) was validated with LANDSAT-7ETM+ thermal data (after resampled to 250 m pixel) of same day (local time 10:00 am, nearby MODIS overpass time 10:15 am, local time) of study area, because of high SR (60 m) data. Since validation using field observation is time and cost effective at the large area with 250 m scale, the effectiveness of the followed merge process may best be assessed by comparison to LANDSAT-7 TIR data over study areas. As revealed in scatter plots between calculated LST and LST of truth image (TIR data of LANDSAT-7 at 250 m), calculated LST was closely related to LST of truth image with $R^2 = 0.74$ (C_1), 0.72 (C_2), 0.71(C_3), and 0.69 (C_4) (Table 2). The results revealed that integrated approach was effective, the accuracy of the output was enhanced. This reveals the fact that vegetation in a higher SR pixel (at 250 m) is usually heterogeneous therefore sharpening of poor SR LST (1 km) is possible. Wonsook et al. (2010) also used TsHARP techniques for downscaling MODIS, LANDSAT-5 TM and ASTER LST data sets with help of NDVI and found good result in evapotranspiration (ET) analysis. In our approach NDVI (at 250 m SR) is major input factor for downscaling LST, in other study (Immerzeel et al., 2009; Bisquert et al., 2016) they also used NDVI (at different SR) for downscaling of LST using some different model but it is clear decision of selection of NDVI as appropriate parameter for downscaling of LST in our study was justified.

The efficiency of TsHARP depends on logic that a healthy correlation always exists between VI (NDVI) and LST. But in case of low NDVI for example, water cover area with low/poor NDVI exhibit low LST, for this case, TsHARP could generate high downscaling errors in those area and in this matter TPS can help us because TPS performs better for various conditions. Thus, TPS could enhanced the efficiency of TsHARP in those areas where NDVI poor/low indicates LST. For this merit of TPS, we merged TsHARP and TPS based on their error estimation hypothesis. The technique with the high error estimation is assign with less weight; therefore, TPS will assign large weights in those areas where TsHARP will act weekly for avoiding high amount of error during downscaling process. Other than TPS, there are many spatial interpolation techniques such as Bilinear, Cubic-convolution and Near-neighbourhood interpolations and are generally used for resampling raster image/data. While smoothing of the resampled raster data using these techniques is slightly inferior to TPS (Chen et al., 2012a,b).

4.2. Result from statistics tests

Our statistics also reveal that merged based downscaling of LST is an effective way to achieve synthetically good resolution thermal data with help of available resolution NDVI (in the desired resolution). Mechri et al. (2014) used genetic particle filter (GPF) approach for downscaling of LST (using NDVI) and found a good

Table 2
statistical test for modeled and observed LST.

Test	Crop area	Crop + Li Sett Area	Crop + Hi Sett Area	Crop + Li+Hi Sett Area
RMSE	0.306	0.215	0.375	0.307
R-RMSE	0.018	0.012	0.022	0.167
NRMSE	0.018	0.013	0.023	0.018
RMSE%	0.047	0.033	0.057	0.016
MAE	0.081	0.025	0.011	0.033
RSR	0.41	0.41	0.40	0.39
d	0.99	0.99	0.99	0.99
R^2	0.74	0.72	0.71	0.63
Multi R	0.80	0.78	0.78	0.76
Adju R	0.75	0.72	0.71	0.71
p	0.000	0.000	0.000	0.000

Li = Light, Hi = High, Sett. = Settlements.

synthetical resolution LST with RMSE = 0.3 (RMSEprior = 1.2 and RMSEposterior = 0.3), which is similar to our result (RMSC for full set data 0.307, Table 2) which shows that our selection of NDVI (as a main factor) for downscaling process is justified. Gao et al. (2012) used mean absolute errors (MAE) statistical test to scale the error in downscaling of LST using data mining sharpener (DMS) approach for the complex terrain and found variation in MAE from 0.78 to 1.67 for downscaling ratios of 1 (250 m) to 4 (1000 m), between the SR of the shortwave (VIR/NIR) and TIR band. This MAE value (0.78) is higher than our MAE (0.081–0.011) for plane terrain area. This difference may be due to the fact that energy conservation enforcement is obtained when LST residuals are incorporated, especially for the C_1, C_3 and complex terrain sites (Gao et al., 2012).

The efficacy of purposed integration approach to improve LST estimation was validated using the LANDSAT-7ETM+ TIR dataset. The results of statistical tests (for validation) are tabulated in Table 2. From this table it can be concluded that the proposed merging of sharpening process has good coefficient of determination (R^2) and low RMSE. The sharpening LST map (at 250 m) is of good accuracy than the 1 km LST from MODIS data and this sharpening method is effective.

Fig. 10 shows the variation of R^2 varies with land types or category at the same time. The coefficient of determination is not much different for different land classes with respect to union of class (Fig. 10b). The highest R^2 (0.74) found for C_1 area in study area, and then R^2 (0.72) for C_2 and then C_3 with R^2 of 0.71. In the category of C_3 R^2 is slightly which may be due to high LST dominant area. From Table 2 'd' given degree of model prediction error and its value varies between zero to one. Value of one reveal an ideal agreement between the observed and model (merged model) predicted values, and zero shows not matching with observed data (LST from LANDSAT-7ETM+). For proposed process, d values in all cases (all classes) are same ($1 \approx 0.99$), that is revealing model (TsHARP + TSP) capable to simulating observed values (from LANDSAT-7ETM+) successfully. R-RMSE (Rawat et al., 2013, Bala et al., 2016) standardizes the RMSE computed LST from TsHARP + TSP model with respect to the observed LST value from LANDSAT-7 at different land bin of category. The advantage of R-RMSE over RMSE, assigns equal weight to overestimation or underestimation of the statistics. From table 2, R-RMSE (0.018 (C_1), 0.012 (C_2), 0.022 (C_3) and 0.67 (C_4)) reveals that model is working well for simulating LST with references to LANDSAT-7. In order to compare RMSE at different category (C_1, C_2, C_3, and C_4), it was normalized to mean of observed LST values and thus normalized RMSE (NRMSE) is calculate. Table 2, NRMSE test also shows model is acceptable due to low values. %RMSE statistics estimates error in predicted values (or model value), the least values of these observed LST, the closer is the model's LST. Ideally, % RMSE values of zero would mean that the observed LST is the same as the model's LST. Generally, the desirability of having zero or low values of %RMSE depends on how close the observed values are. Therefore to compare the closeness of LSTs (from model and observed), percentage root mean square error (% RMSE) are measured and we found modelled and observed LST are nearest (Table 2) for each category of C_n (n = 1, 2, 3, 4). RSR standardizes RMSE using SD (standard deviation) in observations, and it combines both an error index RMSE and SD (Chu and Shirmohammadi, 2004; Singh et al., 2004). RSR values of zero (optimal) would mean that the zero RMSE and perfect simulation by model. Therefore lower RSR (Table 2) shows lower the RMSE and reveal a good simulation with respect to observed LST. MAE statistical test is also used for showing how far model (TsHARP + TSP) LST are from observed LST from LANDSAT-7ETM + and MAE is a more natural calculation of average error and (unlike RMSE) is unambiguous (Rawat et al., 2013; Bala et al., 2016). From Table 2, MAE values (0.081(C_1), 0.025 (C_2), 0.011 (C_3) and 0.033 (C_4)) shows proposed model is acceptable due to less average error and unambiguous in prediction.

5. Conclusions

TIR data provides vital information for land surface energy fluxes and ET, and for near real time agriculture drought monitoring. LST data at fine resolution are required for field scale applications, TIR imagery is normally acquired at a low resolution compared to VIR (visual infrared region) and NIR (near infrared region) spectral bands. Integration of two models (TsHARP and TPS) for remote sensing data sharpening ways has been developed to sharpen TIR data using VIR/NIR reflectance. The analyses of the sharpening method was explored in this paper and were conducted using LST and reflectance data from the MODIS and represent the improved LST maps at high SR (250 m). The application of sharpening of LST data from different sensor may be affected by numerous factors such as the date/time differences, the number of spectral bands available for sharpening, differences in data quality and geo-referencing accuracy. Therefore preference of same sensor product for sharpening of LST data is desirable to avoid errors.

References

Agam, N., Kustas, W.P., Anderson, M.C., Li, F., Neale, C.M.U., 2007a. A vegetation index based technique for spatial sharpening of thermal imagery. Remote Sens. Environ. 107, 545–558.

Agam, N., Kustas, W.P., Anderson, M.C., Li, F., Colaizzi, P.D., 2007b. Utility of thermal sharpening over Texas high plains irrigated agricultural fields. J. Geophys. Res. Atmos. 112. https://doi.org/10.1029/2007JD008407.

Bala, A., Rawat, K.S., Misra, A., Srivastava, A., 2015. Vegetation indices mapping for Bhiwani district of Haryana (India) through LANDSAT-7ETM+ and remote sensing techniques. J. Appl. Natural Sci. 7 (2), 874–879.

Bala, A., Rawat, K.S., Mishra, A.K., Srivastava, A., 2016. Assessment and Validation of Evapotranspiration using SEBALalgorithm and Lysimeter data of IARI Agricultural Farm, India. Geocarto Int. https://doi.org/10.1080/10106049.2015.1076062.

Bindhu, V.M., Narasimhan, B., Sudheer, K.P., 2013. Development and verification of a non-linear disaggregation method (NL-DisTrad) to downscale MODIS land surface temperature to the spatial scale of Landsat thermal data to estimate evapotranspiration. Remote Sens. Environ. 135, 118–129.

Bisquert, M., Sánchez, J.M., Caselles, V., 2016. Evaluation of disaggregation methods for downscaling MODIS land surface temperature to landsat spatial resolution in Barrax Test Site. IEEE J. Selected Topics Appl. Earth Obs. Remote Sensing. https://doi.org/10.1109/JSTARS.2016.2519099.

Boer, E.P.J., de Beurs, K.M., Hartkamp, A.D., 2001. Kriging and thin plate splines for mapping climate variables. Int. J. Appl. Earth Obs. Geoinf. 3, 146–154.

Borra-Serrano, I., Peña, J.M., Torres-Sánchez, J., Mesas-Carrascosa, F.J., López-Granados, F., 2015. Spatial quality evaluation of resampled unmanned aerial vehicle-imagery for weed mapping. Sensors 15, 19688–19708. https://doi.org/10.3390/s150819688.

Chen, C., Li, Y., 2012a. A robust method of thin plate spline and its application to DEM construction. Comput. Geosci. 48, 9–16.

Chen, X., Yamaguchi, Y., Chen, J., Shi, Y., 2012b. Scale effect of vegetation-index-based spatial sharpening for thermal imagery: a simulation study by ASTER data. IEEE Geosci. Remote Sens. Lett. 9, 549–553.

Chu, T.W., Shirmohammadi, A., 2004. Evaluation of the SWAT model's hydrology component in the piedmont physiographic region of Maryland. Trans. ASAE 47 (4), 1057–1073.

Galianoa, V.R., Iguzquiza, E.P., Castilloc, M.S., Olmoa, M.C., Rivas, M.C., 2012. Downscaling Landsat 7 ETM+ thermal imagery using land surface temperature and NDVI images. Int. J. Appl. Earth Obs. Geoinform. 18, 515–527.

Gao, F., Kustas, W.P., Anderson, M.C., 2012. A data mining approach for sharpening thermal satellite imagery over land. Remote Sens. 4, 3287–3319. https://doi.org/10.3390/rs4113287.

Immerzeel, W.W., Rutten, M.M., Droogers, P., 2009. Spatial downscaling of TRMM precipitation using vegetative response on the Iberian Peninsula. Remote Sensing Environ. 113, 362–370.

Mechri, R., Ottlé, C., Pannekoucke, O., Kallel, A., 2014. Genetic particle filter application to land surface temperature downscaling. J. Geophys. Res. Atmos. 119, 2131–2146. https://doi.org/10.1002/2013JD020354.

Rawat, K.S., Mishra, A.K., Kumar, R., Singh, J., 2012. Vegetation Condition Index pattern (2002–2007) over Indian Agro-Climate Regions, using of GIS and SPOT Sensor NDVI Data. J. Appl. Nat. Sci. 4 (2), 214–219.

Rawat, K.S., Mishra, A.K., Sehgal, V.K., Ahmed, N., Tripathid, V.K., 2013. Comparative evaluation of horizontal accuracy of elevations of selected ground control points from ASTER and SRTM DEM with respect to CARTOSAT-1 DEM: A case study ofdistrict Shahjahanpur (Uttar Pradesh), India. Geocarto Int. 28, 439–452.

Rawat, K.S., Mishra, A.K., Bhattacharyya, R., 2016. Soil erosion risk assessment and spatial mapping using LANDSAT7 ETM+, RUSLE and GIS-A case study. Arabian J. Geosci. https://doi.org/10.1007/s12517-015-2157-0.

Singh, J., Knapp, H.V., Demissie, M., 2004. Hydrologic modelling of the Iroquois River watershed using HSPF and SWAT. ISWS CR 2004-08. Champaign, Ill.: Illinois State Water Survey. Available at: www.sws.uiuc.edu/pubdoc/CR/ISWSCR2004-08.pdf. Accessed 2 October- 2016.

Teggi, S., Despini, F., 2014. Estimation of subpixel MODIS water temperature near coastlines using the SWTI algorithm. Remote Sensing Environ. 142, 122–130.

Wang, F., Qin, Z., Li, W., Song, C., Karnieli, A., Zhao, S., 2015. An efficient approach for pixel decomposition to increase the spatial resolution of land surface temperature images from MODIS thermal infrared band data. Sensors 15, 304–330. https://doi.org/10.3390/s150100304.

Wikle, C.K., Berliner, L.M., 2007. A Bayesian tutorial for data assimilation. Phys. D 230, 1–16.

Yang, G., Pu, R., Zhao, C., Huang, W., Wang, J., 2011. Estimation of subpixel land surface temperature using an endmember index based technique: a case examination on ASTER and MODIS temperature products over a heterogeneous area. Remote Sensing Environ. 115 (5), 1202–1219. https://doi.org/10.1016/j.rse.2011.01.004.

Zareie, S., Khosravi, H., Nasiri, A., 2016. Derivation of land surface temperature from Landsat Thematic Mapper (TM) sensor data and analyzing relation between land use changes and surface temperature. Solid Earth Discuss. https://doi.org/10.5194/se-2016-22.

Zhan, W., Chen, Y., Zhou, J., Wang, J., Liu, W., Voogt, J., Zhu, X., Quan, J., Li, J., 2013. Disaggregation of remotely sensed land surface temperature: Literature survey, taxonomy, issues, and caveats. Remote Sens. Environ. 131, 119–139.